Science Advances
AAAS

advances.sciencemag.org/cgi/content/full/4/7/eaar7880/DC1

Supplementary Materials for

Anomalous Hall effect derived from multiple Weyl nodes in high-mobility $EuTiO_3$ films

Kei S. Takahashi*, Hiroaki Ishizuka, Tomoki Murata, Qing Y. Wang, Yoshinori Tokura, Naoto Nagaosa, Masashi Kawasaki

*Corresponding author. Email: kei.takahashi@riken.jp

Published 20 July 2018, *Sci. Adv.* **4**, eaar7880 (2018)
DOI: 10.1126/sciadv.aar7880

This PDF file includes:

Section S1. Optimization of the growth condition of $EuTiO_3$ films by changing the flux ratio between TTIP and Eu

Generally, crystal quality of oxide film strongly depends on the stoichiometry, that is, the Eu/Ti ratio in the case of $EuTiO_3$. In the case of MOMBE growth of titanate films such as $SrTiO_3$ and $BaTiO_3$, a wide growth window for stoichiometric film has been found in previous reports.

In this work, we also elucidated the wide growth window for $EuTiO_3$ film. Figure 1S shows 2θ-θ X-ray diffraction (XRD) scans around the LSAT (002) and $EuTiO_3$ (002) peaks (left panels) and atomic force microscope (AFM) images ($2\times2\mu m^2$) (right panels) of $EuTiO_3$ films grown at 900ºC with TTIP/Eu ratios of 50 [(A), (D)], 80 [(B), (E)], and 210 [(C), (F)]. In Fig. 1S(B), the film peak can be assigned to the (002) peak of tetragonal $EuTiO_3$ accompanied with clear Laue fringes originating from the flat surface and interface, while the Laue fringes for both TTIP/Eu = 50 [Fig. 1S(A)] and 210 [Fig. 1S(C)] are weak. In addition, a peak of secondary phase can be found around 42º in Fig. 1S(A) and tiny peak shift to higher angle of (002) peak of $EuTiO_3$ is seen in Fig. 1S(C). In AFM images, the TTIP/Eu ratio dependence can be also found. Figure 1S(E) exhibits a step-and-terrace structure. The step height is about 4 Å, which corresponds to the height of a single $EuTiO_3$ unit cell. However, the surface of the film with TTIP/Eu = 50 in Fig. 1S(D) is rougher and that with TTIP/Eu = 210 in Fig. 1S(F) shows island structures. Figure 2S(A) shows the TTIP/Eu ratio dependence of the c-axis lattice constant of $EuTiO_3$ films grown by MOMBE. Taking account of the results of XRD scans and AFM images in Fig. 1S, the growth window for stoichiometric $EuTiO_3$ film locates between TTIP/Eu = 60 and 100. The c-axis lattice constant of stoichiometric MOMBE film turns out to be 3.931 Å, which is smaller than that of the previously reported value grown by PLD, denoted as dotted line (3.940 Å). This difference is presumably due to the nonstoichiometry in PLD films. Figure 2S(B) depicts the asymmetric reciprocal space

mappings around the $EuTiO_3$ (103) and LSAT (103) XRD peaks for the film grown with TTIP/Eu = 80, indicating that the in-plane lattice constant is locked to that of the substrate.

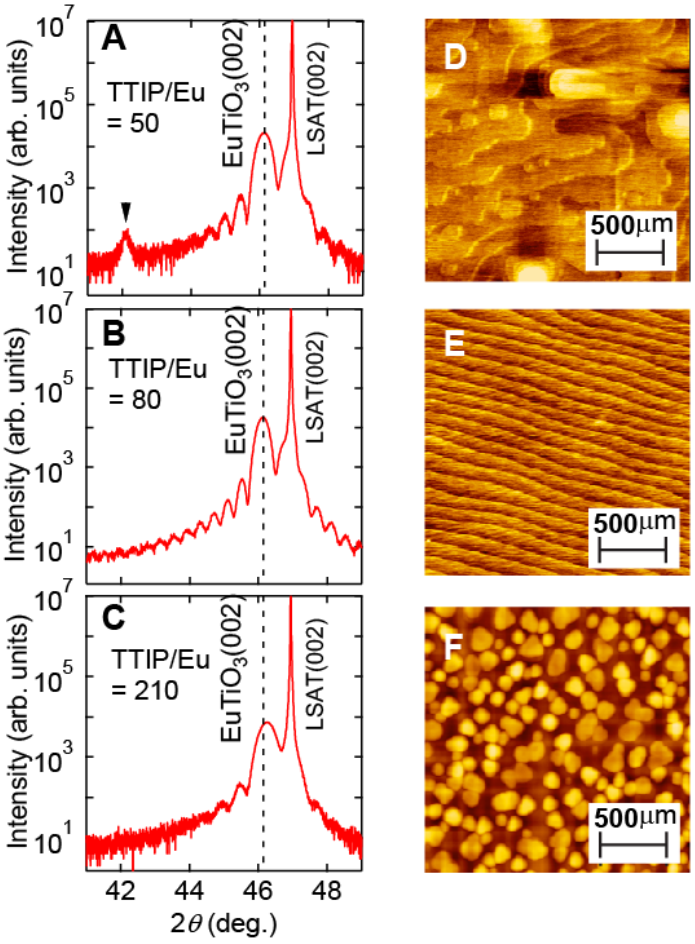

Fig. S1. Structure characterizations of $EuTiO_3$ films on LSAT (001) substrates grown at various TTIP/Eu ratios. 2θ–θ XRD scans for the (002) peak of $EuTiO_3$ and (002) peak of LSAT (left panels) and AFM images ($2 \times 2\mu m^2$) of $EuTiO_3$ films (right panels). Films were grown at TTIP/Eu ratios of: (A), (D) 50, (B), (E) 80, and (C), (F) 210.

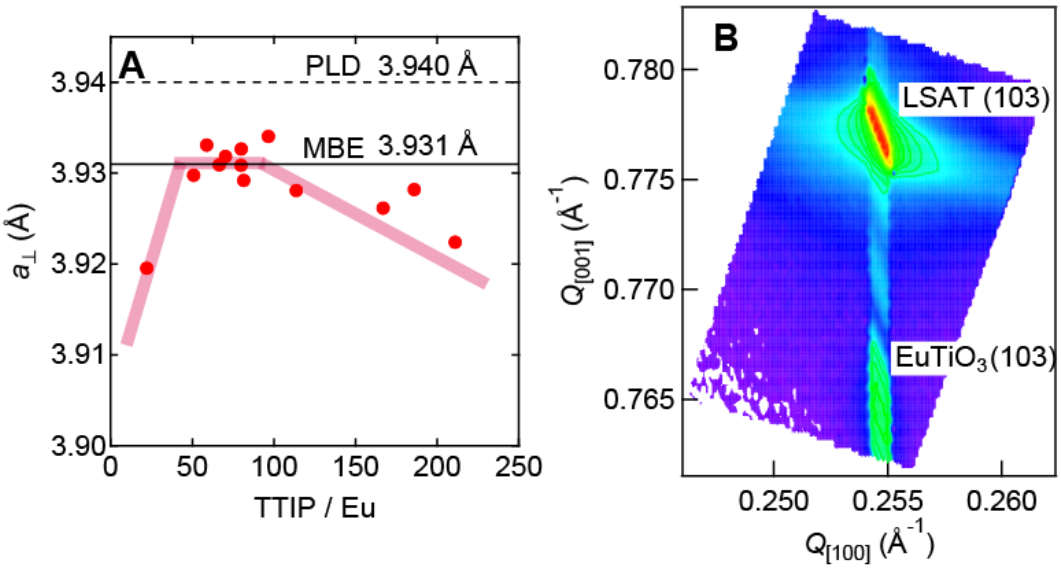

Fig. S2. Tetragonal distortion of $EuTiO_3$ film on LSAT (001) substrate. (A) c-axis (out-of-plane) lattice constant for $EuTiO_3$ films on LSAT(001) as a function of TTIP/Eu ratio. Between TTIP/Eu = 50 and 100, stoichiometric and strained $EuTiO_3$ films can be grown with a steady out-of-plane lattice constant of 3.931 Å. Broken line indicates that for PLD films. (B) Reciprocal space mapping for the asymmetric (103) peak of $EuTiO_3$ and (103) peak of LSAT.

Section S2. Temperature dependence of magnetization

To check the magnetic transition in the $EuTiO_3$ film on LSAT, temperature dependence of magnetization was measured. For both curves with the magnetic field applied parallel to in-plane and out-of-plane axes, clear anomalies can be seen around 5.5 K, corresponding to the antiferromagnetic transition.

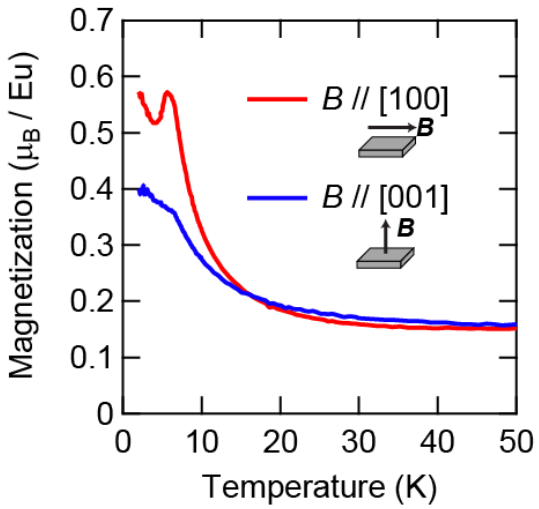

Fig. S3. Magnetization property. Temperature dependence of magnetization at 500 Oe for a $EuTiO_3$ film on LSAT(001). The magnetic field is applied parallel to in-plane [100] (red line) and out-of-plane [001] (blue) axes.

Section S3. Anomalous Hall conductivity σ_{xy} for La-doped ETO films

Here, anomalous Hall conductivity estimated by $\sigma_{\mathrm{AHE}}(B) = \frac{\rho_{\mathrm{AHE}}(B)}{\rho_{\mathrm{AHE}}(B)^2 + \rho_{xx}(B=0)^2}$ is plotted for various carrier density films. As discussed in main text, a clear non-linear part below the saturation magnetic field can be observed. Interestingly, the curvature of non-linear part changes the sigh twice from negative to positive, and to negative as the carrier density increases, whereas the saturation value of anomalous Hall conductivity changes the sign once.

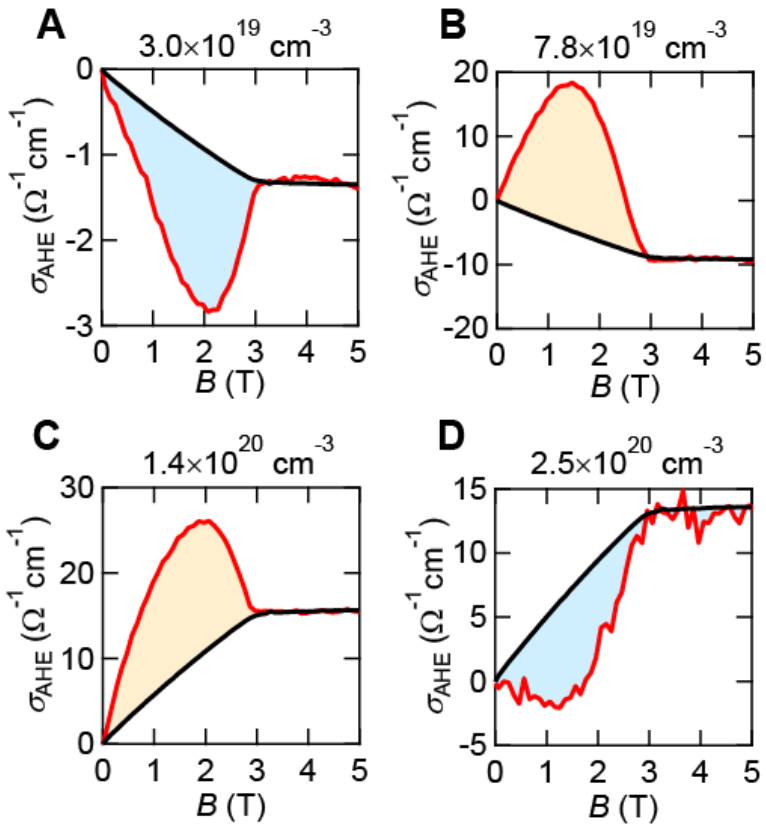

Fig. S4. Magnetic field dependence of anomalous Hall conductivity. Anomalous Hall conductivity as a function of magnetic field at 2 K for the La doped ETO films with n = 3.0×10^{19} cm^{-3} (A), 7.8×10^{19} cm^{-3} (B), 1.4×10^{20} cm^{-3} (C), and 2.5×10^{20} cm^{-3} (D).

Section S4. Berry curvature distribution of the Luttinger model

We here study the distribution of the Berry curvature in the four conduction bands of Ti 3*d* electrons. As discussed in the main text, the effective model is described by the Luttinger model with uniaxial anisotropy. The top (fig. S5B) and bottom (fig. S5E) band of the model shows a relatively simple distribution of the Berry curvature flux with a source and a drain reflecting the Weyl nodes in the bands. On the other hand, the two bands in the middle (fig. S5C and S5D) shows a complicated distribution of the Berry curvature reflecting six Weyl nodes on the bands.

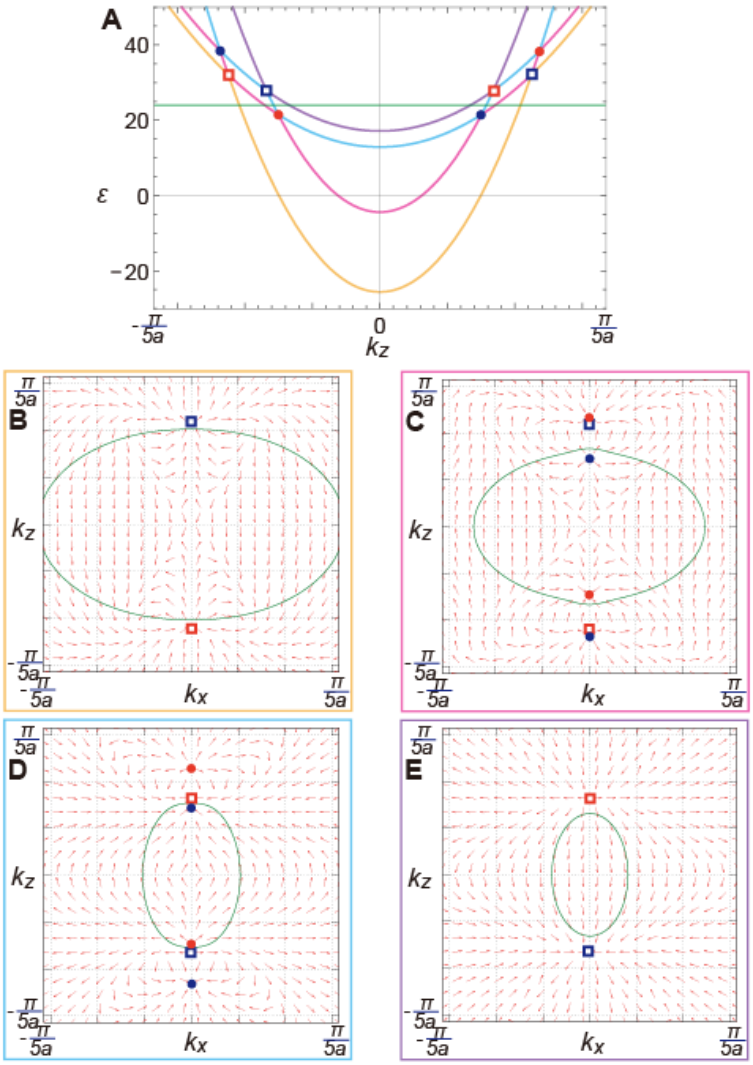

Fig. S5. Band structure and Berry curvature. (A) The band structure of the four bands in the effective Hamiltonian under magnetic field. Four bands are colored in different colors. The green straight line is the Fermi level for $\mu = 24$ meV, and the circles (squares) are the Weyl (double Weyl) points in the Brillouin zone. The red (blue) symbols are nodes with positive (negative) chirality. (B)−(E) Berry curvature for the four bands on the $k_y = 0$ plane. The green lines are the Fermi surfaces at $\mu = 24$ meV. The color of the box corresponds to the color of the bands in (A). The dots and squares are Weyl and double Weyl points on each band, respectively. Red symbols are for the nodes with positive chirality and the blues are for negative ones. The green circle is the Fermi surface for $\mu = 24$ meV. All results are for $t = 300$ meV, $\delta t = -100$ meV, $\mathrm{V_{tetra}} = 45$ meV, and $\theta = -\pi/4$.